

# Radiatively and thermally driven self-consistent bipolar outflows from accretion discs around compact objects

Rajiv Kumar<sup>1\*</sup>, Indranil Chattopadhyay<sup>1</sup>, Samir Mandal<sup>2</sup>

<sup>1</sup>*Aryabhata Research Institute of Observational Sciences (ARIES), Manora Peak, Nainital – 263002, India*

<sup>2</sup>*Indian Institute of Space Science & Technology (IIST), Trivandrum, India.*

Accepted —. Received —; in original form —

## ABSTRACT

We investigate the role of radiative driving of shock ejected bipolar outflows from advective accretion discs in a self consistent manner. Radiations from the inner disc affects the subsonic part of the jet while those from the pre-shock disc affects the supersonic part, and there by constitutes a multi stage acceleration process. We show that the radiation from the inner disc not only accelerate but also increase the mass outflow rate, while the radiation from the pre-shock disc only increases the kinetic energy of the flow. With proper proportions of these two radiations, very high terminal speed is possible. We also estimated the post-shock luminosity from the pre-shock radiations, and showed that with the increase of viscosity parameter the disc becomes more luminous, and the resulting jet simultaneously becomes faster. This mimics the production of steady mildly relativistic but stronger jets as micro-quasars moves from low hard to intermediate hard spectral states.

**Key words:** hydrodynamics, radiation hydrodynamics, black hole physics, accretion, accretion discs, jets and outflows

## 1 INTRODUCTION

Jets are ubiquitous and are observed to accompany a variety of astrophysical objects such as, stellar-mass and super-massive black hole candidates, neutron stars, white dwarfs, young stellar objects (YSOs) etc. These outflows exhibit different physical scales and power *e.g.*, at one extreme, AGNs have jets with typical sizes  $\sim$  few Kpc to few  $\times$  100 Kpc, jet velocities comparable to  $c$  (where  $c$  is the light speed), luminosity range  $10^{43-48}$  erg/s and central mass in the range  $10^{6-9} M_{\odot}$  (where  $M_{\odot}$  is the mass of Sun), while in the other extreme, YSO jets have typical size  $\leq$  1pc, outflow velocity  $< 10^{-3}c$ , luminosity range  $(0.1 - 2) \times 10^{36}$  erg/s, and emerge from protostars with mass  $\sim 1M_{\odot}$ . In other words, only jets around compact objects are truly relativistic. Jets around black hole candidates, be it from AGNs or micro-quasars, are shrouded in mystery. Since black holes do not have hard surface and/or any atmosphere, therefore jets can only originate from the matter accreting onto it. Moreover, the terminal speed of jets from around compact objects, though relativistic, but can vary widely too. For *e.g.*, jets around GRS 1915+105 or M87 exhibit terminal speed above ninety percent the speed of light (Mirabel & Rodriguez 1994; Biretta 1993), while the jet around SS433 is merely around  $0.26c$  (Margon 1984). Therefore, not only there is no consensus about the origin of jets, even the acceleration mechanism of jets are not well understood.

There are few interesting properties of jets around compact objects. Junor *et al.* (1999) showed that the jet around M87 seems to originate within a region less than  $100 r_s$  ( $r_s = 2GM/c^2$  is the Schwarzschild radius) around the central object. In other words, entire accretion disc do not participate in generation of jets, but only the inner region of the accretion disc participate in jet generation. Although the connection between jet states and spectral states of the accretion disc has not been conclusively established for massive black hole candidates like the AGNs, but for micro-quasars, this connection has firmly been established (Gallo *et al.* 2003; Fender *et al.* 2010; Rushton *et al.* 2010). Persistent, quasi steady, mildly relativistic jets are observed in ‘hard spectral state’ (maximum power in the hard power law tail) of the accretion disc. The jet seems to get stronger as the spectral state of accretion disc moves to the intermediate states. And truly relativistic jet blobs are generated

\* E-mail: rajiv.k@aries.res.in (RK); indra@aries.res.in (IC); samir@iist.ac.in (SM)

during state transition to the steep power law state. No jet activity is observed in the canonical soft state (maximum power in modified black body component) (Gallo *et al.* 2003; Fender & Beloni 2004; Rushton *et al.* 2010). Such close correlation of jet with the radiative states of the disc, points to the fact that the accretion disc physics is responsible for jet generation.

Matter accreting onto a compact object should possess some angular momentum and due to differential rotation some form of anomalous viscosity too. The first viscous disc model seriously considered by the community is the standard thin disc (Shakura & Sunyaev 1973; Novikov & Thorne 1973), although thin disc's inability to explain the origin of power-law photons, as well as, the theoretical inconsistencies like *ad hoc* inner boundary condition, remained an overbearing concern. It was understood that a source of hot electron distribution *i.e.*, a Comptonizing corona, is required to explain the hard power law photons in the spectra of black hole candidates (Sunyaev & Titarchuk 1980). Since the boundary condition of black hole accretion is necessarily transonic, disc models with significant advective term gained popularity. The most popular model among the advective disc models was known as ADAF or advection dominated accretion flow (Narayan *et al.* 1997). This model is characterized by a single sonic point close to the horizon and subsonic elsewhere. However, it has been shown earlier that multiple sonic point may exist for inviscid rotating flow (Liang & Thompson 1980), and was confirmed that this is also true for dissipative advective accretion discs (Chakrabarti 1996; Lu *et al.* 1999; Chakrabarti & Das 2004). And therefore it was shown by various authors that ADAF is only a subset of general advective solution (Lu *et al.* 1999; Das *et al.* 2009; Kumar & Chattopadhyay 2013). General advective solutions which admits multiple sonic points may harbour standing or time-dependent shock solutions (Fukue 1987; Chakrabarti 1989, 1996; Fukumura & Tsuruta 2004; Lanzafame *et al.* 2008; Chattopadhyay 2008; Nagakura & Yamada 2009; Chattopadhyay & Chakrabarti 2011). Shock in accretion has some interesting consequences, for *e.g.*, the post shock hot electrons may inverse Comptonize soft photons to produce the non-thermal hard radiation tail (Chakrabarti & Titarchuk 1995; Chakrabarti & Mandal 2006). A dominant shock associates with a low supply of soft photons from external Keplerian disc, and the hot post-shock region inverse-Comptonizes the intercepted photons and produces the low/hard state. And an increased supply of Keplerian matter means supply of extra soft photons to cool down the post-shock region which results in weakening of, or, complete removal of the shock to produce the canonical high/soft state. In fact, the hardness intensity diagram (HID) of GRO J 1655-40 was well explained by shocked accretion disc (Mandal & Chakrabarti 2010). These studies also showed that the steady state shock solutions are possible in a limited range of the parameter space, while oscillating or time dependent shocks are possible for a wide range of parameters or boundary conditions (Molteni *et al.* 1996b; Nishikawa *et al.* 2005; Nagakura & Yamada 2009). And since these post-shock region also emits high energy radiations, therefore quasi-periodic oscillation of the shocked disc will give rise to quasi-periodic oscillation in hard radiations as well, and was furthered as a model for quasi-periodic oscillations or QPOs (Molteni *et al.* 1996b; Chakrabarti & Manickam 2000; Nishikawa *et al.* 2005; Nagakura & Yamada 2009). It was shown from observations that the spectral index increases (hard to soft transition) with the increase of QPO frequency, but remarkably the spectral index saturates (indicating the attainment of high/soft state) and then there are no QPO detected (Shaposhnikov & Titarchuk 2009). The evolution of the QPO frequency with the spectral state for outburst sources like XTEJ1550-654, GRO 1655-40 etc, has been explained well with a model of inward drift of oscillating shock which translates into a spectral state transition from low/hard to intermediate hard. And the final disappearance of QPO with the disappearance of the inner disc or the post-shock disc (Chakrabarti *et al.* 2008, 2009). And it has been shown that indeed for the same outer boundary condition, the shock drifts inwards with the increase of the viscosity parameter (Chattopadhyay & Das 2007; Kumar & Chattopadhyay 2013). This implies that, with the increase of viscosity the pre-shock disc size increases, which increases the supply of soft photons. As the post-shock disc gets reduced, eventually the total output of the thermal Comptonization (dominant spectra in low/hard state) decreases too. And since according to the advective accretion disc model, oscillation of post-shock disc gives rise to QPO, so the decrease of shock location increases the QPO frequency, until the shock itself disappears. Hence the transition from hard to soft state, or in other words, the increase of spectral index should be correlated with the increase of QPO frequency, and finally the spectral index saturates (Titarchuk & Fiorito 2004; Shaposhnikov & Titarchuk 2007) as the contribution to the radiation from post-shock disc becomes negligible (Chakrabarti *et al.* 2008).

In our previous paper (Kumar & Chattopadhyay 2013), we have presented all possible advective viscous accretion solutions, including shocked and shock free solutions. A shocked accretion disc is more interesting, because the post-shock disc being hot can drive bipolar-outflows (Molteni *et al.* 1996a; Chakrabarti 1999; Chattopadhyay & Das 2007; Das & Chattopadhyay 2008; Kumar & Chattopadhyay 2013). Since shock forms typically at  $x_s \lesssim \text{few} \times 10r_s$ , so the assertion that jet base is the inner part of the disc, favours the observational evidence from M87 that jet base is indeed  $< 100r_s$  (Junor *et al.* 1999; Doleman *et al.* 2012). Since it has also been shown that AGNs are just a scaled up version of the galactic black holes (McHardy *et al.* 2006), therefore, following the above evidence one may argue that even for galactic black holes the jet base should be close to the central object. However, it is not just theoretical expectation that the inner region around AGNs and micro-quasars should be similar, therefore, the jet base for microquasars too would be close to the horizon. Even in case of galactic Black Hole Candidates (BHC), the detection of strong radio flares (read jets) with simultaneous disappearance of QPOs and the absence of the Comptonized component, points out to the fact that the same region which gave rise to the Comptonized component and generated the QPO has been ejected as relativistic jets (Feroci *et al.* 1999; Vadawale *et al.* 2001). The shocked accretion disc model seems to satisfy all these criteria, starting with the direct evidence of M87 jet orig-

inating close to the black hole, the connection between growth of QPO frequency, Comptonized component and the radio flare, to the disappearance of jet activity in the soft state (no or very weak shock). Das *et al.* (2001) showed (Fig. 5 of their paper) that the correlation between thermally driven jets from shocked accretion discs and the spectral states from the same discs seems to follow the conclusions of observations of 10 microquasars (Gallo *et al.* 2003). Since post-shock disc produces the jets therefore when shock is absent or very weak, jets disappear mimicking the soft state. But thermally driven jets can achieve terminal speed up to  $v_\infty \lesssim [2\{a_b^2/(\gamma - 1) - \Phi_b\}]^{1/2}$ , where  $a_b$  is the sound speed at the base, which for a shocked disc is the sound speed of the post-shock disc, and  $\Phi_b$  is the gravitational potential at the jet base. Now the maximum sound speed physically possible is  $a_{\max} = c/\sqrt{3}$ , and that the value of  $\Phi_b$  is quite significant because the jet base is rather close to the horizon (Junor *et al.* 1999). Given these facts, the expression of terminal speed given above indicates that, truly relativistic jet terminal speed is not possible by only thermal driving. Furthermore, jet states are correlated with the hard spectral states of the accretion disc, therefore, can the disc radiation accelerate the outflowing jet material? In this respect, one may raise the issue that jet activities are not always observed during the state transition, which might be due to the lack of availability of simultaneous X-ray and radio/infra-red measurements. However, Gallo *et al.* (2003) studied about 10 sources to draw the correlation between jet activity with the hard states, and the conclusion that jets are not seen during the canonical soft states. We would therefore like to study the interaction of radiations from the hard/hard intermediate states with the emanating jet, or in our parlance, the acceleration of jets with the radiation from a shocked disc, and how this radiative acceleration of jets is influenced with the change in viscosity parameter of the disc. It is to be remembered that, since we are investigating the disc in steady state, we are actually studying the generation and acceleration of steady, mildly relativistic jets generally associated with hard to hard intermediate states. The strong radio flares associated with relativistic blob ejections during hard intermediate to soft intermediate state transition (Miller-Jones *et al.* 2012) is intrinsically a time dependent phenomenon and has not been addressed in this paper. Since we have not incorporated all the physical aspects to mimic the transient phenomena, in this limited sense the results depend on the model assumptions.

Interaction of the disc radiation with the outflowing matter has been followed by many authors. Icke (1980) studied radiative acceleration of jets above a Keplerian disc, but in absence of radiation drag. Sikora & Wilson (1981) showed that radiation drag is important for jets powered by radiation from a thick accretion disc (Lynden-Bell 1978). Including radiation momentum deposition on an axial particle jet illuminated by an infinite thin disc in presence of drag term, Icke (1989) showed that the upper limit of the terminal speed is around 45% of  $c$ . Investigations on radiatively driven jets were extended by Fukue (1996); Fukue *et al.* (2001) to generate relativistic terminal speeds for particle jets. Moreover, the interaction of radiations from shocked accretion disc and jets were studied too (Chattopadhyay & Chakrabarti 2000, 2002, 2003; Chattopadhyay *et al.* 2004; Chattopadhyay 2005). Since shocked discs have two radiation sources, namely, the post-shock and pre-shock disc, therefore the redistribution of radiative power amongst these sources, could efficiently accelerate the jet around its axis. However, jets studied in the above mentioned papers were decoupled from the disc. In this paper we would like to study radiatively driven jet which is generated self consistently from the underlying accretion disc. In other words, we combine the accretion-ejection physics described by Kumar & Chattopadhyay (2013) with the effect of radiative momentum deposition on the jets as shown by Chattopadhyay & Chakrabarti (2002).

In the next section, we present the simplifying assumptions and equations of motion. In section 3, we present the methodology of solution. And in the last section we present the solutions and discussion.

## 2 EQUATIONS OF MOTION AND ASSUMPTIONS

In this paper, we have assumed the axis-symmetric disc-jet system to be in steady state. The black hole is assumed to be non-rotating described by the pseudo-Newtonian potential introduced by Paczyński & Wiita (1980). The viscosity prescription in the accretion disc is described by the Shakura-Sunyaev  $\alpha$  viscosity. The jets are tenuous and should have less differential rotation than the accretion disc, as a result the viscosity in jets can be ignored. To negate any resulting torque, the angular momentum at the jet base is assumed same as that of the local value of angular momentum of the disc. We estimate the radiative moments, namely, the radiative energy density, flux, and radiative pressure from the disc. The jets being optically thin are subjected to radiation force including the drag terms. Figure 1, shows the schematic diagram of the disc-jet system, where the pre-shock, post-shock disc and the jet are clearly marked. The black hole is at BH. The accretion disc occupies the space on or about the equatorial plane, and the jet flow geometry is about the axis of symmetry. We have used the geometric unit system where,  $2G = M = c = 1$  ( $M$  is the mass of the black hole,  $G$  is the Gravitational constant). Therefore, in this representation the unit of length is, the Schwarzschild radius or  $r_s = 2GM/c^2$ , the unit of mass is that of the central black hole  $M$ , and that of time is  $r_s/c = 2GM/c^3$ , respectively, consequently the unit of speed is  $c$ .

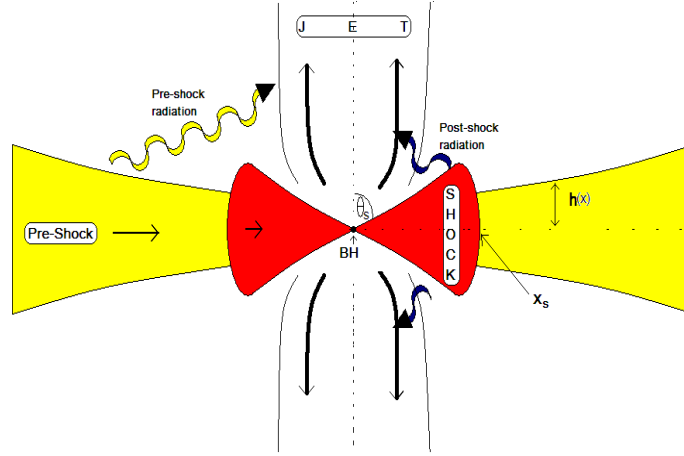


**Figure 1.** Cartoon for disc-jet system. BH is the acronym for black hole. Both pre-shock and post-shock disc shines radiation on the bipolar jet. The shock location  $x_s$ , the axis (vertical dotted) and equatorial plane (horizontal dotted) are shown. The half height  $h(x)$ , and the opening half angle  $\theta_s$  of the funnel like region between the inner torus is shown.

## 2.1 Equations of motion for accretion and ejection system

Since we are investigating self-consistent accretion-ejection system, we should present the governing equations together. However, since the accretion and jets follow different flow geometries, we present them separately. In section 2.1.1, we present equations of motions, which when solved gives us the accretion solution. In section 2.1.2, the equations governing the jet solution are presented. And finally in section 2.2, we present the solution procedure, *i.e.*, how a jet solution is simultaneously obtained from accretion disc through shocks.

### 2.1.1 Equations governing the accretion disc

The equations of motion of the accreting matter around the equatorial plane, in cylindrical coordinates  $(x, \phi, z)$ , have been extensively presented in the literature (Chakrabarti 1996; Kumar & Chattopadhyay 2013). Here we give a brief account of them.

These equations are the radial momentum equation, the accretion rate equation for a disc in vertical equilibrium, the angular momentum conservation equation and the entropy generation equation, and they are

$$u \frac{du}{dx} + \frac{1}{\rho} \frac{dp}{dx} + \frac{1}{2(x-1)^2} - \frac{\lambda^2(x)}{x^3} = 0, \quad (1)$$

$$\dot{M} = 2\pi \Sigma u x, \quad (2)$$

$$u \frac{d\lambda(x)}{dx} + \frac{1}{\Sigma x} \frac{d(x^2 W_{x\phi})}{dx} = 0 \quad (3)$$

$$\Sigma u T \frac{ds}{dx} = Q^+ - Q^-. \quad (4)$$

The local variables  $u$ ,  $p$ ,  $\rho$  and  $\lambda$  in the above equations are the radial velocity, isotropic pressure, density and specific angular momentum of the flow, respectively. Here,  $\Sigma = 2\rho h$  is vertically integrated density with  $h$  being the local disc height from equatorial plane and  $W_{x\phi}$  is the viscous stress tensor. Moreover,  $s$ ,  $T$  are the entropy density and the local temperature respectively. The local heat gained (due to viscosity) and lost by the flow are given by  $Q^+ = W_{x\phi}^2/\eta$  and  $Q^-$ . The viscous stress, the local half height and the sound speed are given by

$$W_{x\phi} = \eta x \frac{d\Omega}{dx}, \quad h(x) = \sqrt{\frac{2}{\gamma}} a x^{1/2} (x-1), \quad a = \sqrt{\frac{\gamma P}{\rho}} \quad (5)$$

where,  $\eta = \rho \nu h$  is the dynamic viscosity coefficient,  $\nu = \alpha a^2 / (\gamma \Omega_k)$  is the kinematic viscosity,  $\alpha$  is the Shakura-Sunyaev viscosity parameter,  $\Omega$ ,  $\Omega_k$  and  $\gamma$  are the local angular velocity, local Keplerian angular velocity and adiabatic index, respectively. Here, all the variables have been made dimensionless by employing the unit system mentioned above section 2.1, *e.g.*, if  $\tilde{r}$ ,  $\tilde{u}$  etc are dimensional radial coordinate and velocity, then  $x = \tilde{r}/r_s$ ,  $u = \tilde{u}/c$  etc.

Integrating equation (1) with the help of Eq. (2-4), we find another constant of motion called the specific grand energy

(Gu & Lu 2004) of the flow and is given by

$$E = \frac{u^2}{2} + \frac{a^2}{\gamma - 1} - \frac{\lambda^2}{2x^2} + \frac{\lambda_0 \lambda}{x^2} - \frac{0.5}{(x - 1)}, \quad (6)$$

where,  $a$ ,  $\lambda_0$  are local sound speed and the specific angular momentum of the flow on the horizon which is one of the constants of integration.

Using the adiabatic law, the definition of sound speed, and the mass-accretion equation (Eq. 2), entropy-accretion rate is defined

$$\dot{\mathcal{M}}(x) = a^{(2n+1)} u x^{3/2} (x - 1), \quad (7)$$

where  $n = 1/(\gamma - 1)$ .  $\dot{\mathcal{M}}$  is the measure of local entropy and is constant for an inviscid and adiabatic flow.

We rearrange and simplify Eqs. (1-4) to the following forms (see, Kumar & Chattopadhyay 2013 for details),

$$\frac{du}{dx} = f_1(u, a, \lambda, \lambda_0, \alpha, \gamma, x); \quad \frac{d\lambda}{dx} = f_2(u, a, \lambda, \lambda_0, \alpha, \gamma, x); \quad \frac{da}{dx} = f_3(u, a, \lambda, \lambda_0, \alpha, \gamma, x) \quad (8)$$

Since accreting matter at  $x \rightarrow \infty$  is subsonic, and close to the horizon it is supersonic, at some point in between, the flow would become transonic, where  $du/dx \rightarrow 0/0$ . This gives the so-called sonic point conditions or critical point conditions. And at  $x = x_c$  or sonic point, the gradient is calculated by employing L'Hospital rule. The accretion solutions are obtained by solving Eqs. (8) with the help of sonic point conditions.

### 2.1.2 Jet equations of motion

The jet streamline is approximated from the numerical simulations (Molteni *et al.* 1996a), where the jet flows through the funnel wall (FW) and the centrifugal barrier (CB). A detail jet geometry has been described in Kumar & Chattopadhyay (2013). All the jet variables in the equations below have been made dimensionless by dividing the distances with  $r_s$ , velocities with  $c$ , mass with  $M$  etc.

The disc photons accelerate the jet by depositing the radiation momentum onto the jet. Since the jet is optically thin so the radiation actually penetrates the jet. So every fluid parcel of the jet is accelerated by the radiation from behind, but the radiation field ahead also drags and decelerate the parcel. The momentum balance equation of the jet, correct up to first order in velocity, is given by (Mihalas & Mihalas 1984; Chattopadhyay & Chakrabarti 2002)

$$v_j \frac{dv_j}{dr} + \frac{1}{\rho_j} \frac{dp_j}{dr} - \frac{\lambda_j^2}{x_j^3} \frac{dx_j}{dr} + \frac{1}{2(r_j - 1)^2} \frac{dr_j}{dr} = \mathcal{F}_{r_j} - v_j(\mathcal{E}_{r_j} + \mathcal{P}_{r_j}) \quad (9)$$

Here,  $\mathcal{F}_{r_j} = \sigma_T F_{r_j} / m_e c$ ,  $\mathcal{E}_{r_j} = \sigma_T E_{r_j} / m_e$ , and  $\mathcal{P}_{r_j} = \sigma_T P_{r_j} / m_e$ , where,  $\sigma_T$  is the Thompson scattering cross section,  $m_e$  is the electron mass, and  $F_{r_j}$ ,  $E_{r_j}$ ,  $P_{r_j}$  are radiative flux, radiative energy density and radiative pressure, respectively. The streamline is computed as  $r_j = \sqrt{x_j^2 + y_j^2}$ . The first term in r. h. s of Eq. (9) is the acceleration term, while negative terms are the radiative drag term. All the terms with the suffix 'j' represents jet quantities. If  $\mathcal{F}_{r_j} = \mathcal{E}_{r_j} = \mathcal{P}_{r_j} = 0$ , then Eq. (9) can be integrated to give the Bernoulli equation for jet,

$$\mathcal{E}_j = \frac{v_j^2}{2} + \frac{a_j^2}{\gamma - 1} + \frac{\lambda_j^2}{2x_j^2} - \frac{1}{2(r_j - 1)} \quad (10)$$

For purely thermally driven flow  $\mathcal{E}_j$  is a constant of motion, however, for a radiatively driven flow  $\mathcal{E}_j$  is a variable, as we will show later (Figs. 4e, 5e). The jet outflow rate is given by

$$\dot{M}_{out} = \rho_j v_j \mathcal{A}, \quad (11)$$

where  $\mathcal{A}$  is the cross-sectional area of the jet. Since absorption and emission terms in the jet is zero, therefore, it is described by the polytropic equation of state ( $p_j = K_j \rho_j^\gamma$ ). The entropy accretion rate (from Eq. 11) for the jet is given by

$$\dot{\mathcal{M}}_j = a_j^{2n} v_j \mathcal{A}. \quad (12)$$

$\dot{\mathcal{M}}_j$  is a measure of entropy of the jet, and is constant along the jet since heating and cooling is ignored. Equations (9,12) are simplified, to obtain,

$$\frac{dv_j}{dr} = \frac{\mathcal{N}}{\mathcal{D}}, \quad (13)$$

where,

$$\mathcal{N} = \frac{1}{2(r_j - 1)^2} \frac{dr_j}{dr} - \frac{\lambda_j^2}{x_j^3} \frac{dx_j}{dr} - \frac{a_j^2}{\mathcal{A}} \frac{d\mathcal{A}}{dr} - \mathcal{F}_{r_j} + v_j(\mathcal{E}_{r_j} + \mathcal{P}_{r_j}), \quad (14)$$

and,

$$\mathcal{D} = \frac{a_j^2}{v_j} - v_j. \quad (15)$$

The sonic point ( $r_{jc}$ ) condition for jet is obtained for the condition  $r_j \rightarrow r_{jc}$ ,  $dv_j/dr \rightarrow 0/0$ ,

$$v_{jc} = a_{jc} = \frac{-A_2 + \sqrt{A_2^2 - 4A_1A_3}}{2A_1}; \quad (16)$$

where,

$$A_1 = \left[ \frac{1}{\mathcal{A}_c} \left( \frac{d\mathcal{A}}{dr} \right)_{r_c} \right], \quad A_2 = -(\mathcal{E}_{rj} + \mathcal{P}_{rj}), \quad A_3 = \left[ \mathcal{F}_{rj} - \frac{1}{2(r_{jc} - 1)^2} \left( \frac{dr_j}{dr} \right)_{r_c} + \frac{\lambda_{jc}^2}{x_{jc}^3} \left( \frac{dx_j}{dr} \right)_{r_c} \right].$$

The gradient of jet velocity on the sonic point is obtained by L'Hospital rule

$$\left[ \frac{dv_j}{dr} \right]_c = \left[ \frac{dN/dr}{dD/dr} \right]_c. \quad (17)$$

To obtain the jet solutions one has to integrate Eq. 13, with the help of Eqs. (16-17). In this paper we have chosen the adiabatic index to be  $\gamma = 1.4$ , and has been shown to be the typical value close to the black hole (Chattopadhyay & Chakrabarti 2011).

## 2.2 The method to calculate self-consistent accretion-ejection solution

The jet solution is dictated by the accretion solution, and now we discuss how we obtain the self-consistent accretion-ejection solution. The accretion solution depends on the following constants of motion  $E$ ,  $\lambda_0$ , and the viscosity parameter  $\alpha$ . Therefore, our first step is to obtain the accretion solution.

Step 1: Initially we assume no jet *i.e.*,  $\dot{M}_{out} = 0$  and integrate Eqs. (1-4) *i.e.*, Eqs. (8) outwards and find the inner sonic point ( $x_{ci}$ ) iteratively by choosing appropriate  $\dot{\mathcal{M}}$  and simultaneously checking for the sonic point conditions (Eqs. 16-19, of Kumar & Chattopadhyay 2013). The first hurdle to obtain the accretion solution is that although flow parameters are regular but there is a coordinate singularity on the horizon. However, the asymptotic values of  $u(x)$ , and  $\lambda(x)$  very close to the horizon at  $x_{in}$ , are obtained for appropriate values of  $\dot{\mathcal{M}}$  (Becker *et al.* 2008), and are given by,

$$\lambda(x) = \lambda_0 \left[ 1 + \frac{2\alpha}{\gamma r_g} \left( \frac{2}{r_g} \right)^{1/2} \left( \frac{\dot{\mathcal{M}}^2}{2r_g^3} \right)^{\frac{\gamma-1}{\gamma+1}} (x - r_g)^{\frac{\gamma+5}{2\gamma+2}} \right], \quad x \rightarrow 1 \quad (18)$$

and

$$u(x) = u_{ff}(x) \left[ 1 + \frac{2Ex^2 - \lambda_0^2 - (\gamma+1)f(x)}{x^2 u_{ff}^2(x) - (\gamma-1)f(x)} \right]^{1/2}, \quad x \rightarrow 1 \quad (19)$$

where the function  $f(x)$  is  $f(x) = 2x^2(\gamma^2 - 1)^{-1} \left[ \dot{\mathcal{M}}^2 / \{2x^3(x-1)\} \right]^{\frac{\gamma-1}{\gamma+1}}$  and the free fall velocity in the pseudo-Newtonian potential is given by  $u_{ff}(x) = 1/\sqrt{(x-1)}$ . Without any loss of generality we choose  $x_{in} = 1.01$ , and with these asymptotic values at  $x_{in}$  we start the integration of Eqs. 8 and find the sonic points of the accretion solution. All kinds of solutions can be obtained, ranging from solutions passing through one sonic point (ADAF type and for low angular momentum flow BONDI type, see Kumar & Chattopadhyay 2013), to flow solutions harbouring multiple sonic points. Only flows harbouring multiple sonic points can have shocks. Once a flow passes through inner type sonic points  $x_{ci}$ , we integrate the flow equations while checking for the shock conditions (Eq. 20-22) and sonic point conditions to calculate shock location ( $x_s$ ) and outer sonic point ( $x_{co}$ ) simultaneously. The shock conditions are,

$$W_+ + \Sigma_+ u_+^2 = W_- + \Sigma_- u_-^2, \quad (20)$$

$$E_+ = E_-, \quad (21)$$

and the mass flux

$$\dot{M}_+ = \dot{M}_- - \dot{M}_{out} = \dot{M}_- (1 - R_{in}), \quad \text{where } R_{in} = \frac{\dot{M}_{out}}{\dot{M}_-} = \frac{R\rho_j v_j(x_b)\mathcal{A}(x_s)}{2\pi\Sigma_+ u_- x_s}, \quad (22)$$

where  $+$  and  $-$  represents the post-shock and pre-shock quantities, respectively and  $W$  is vertically integrated pressure. Here,  $R = u_-/u_+ = \Sigma_+/\Sigma_-$  is the compression ratio at the shock. If there is no shock then  $R = 1$ , and otherwise  $R > 1$ . As has been mentioned above, the initial accretion solution is obtained by putting  $R_{in} = 0$ .

Step 2: After we obtain the accretion temperature and number density distribution from the accretion solution, we compute the radiative moments  $\mathcal{E}_{rj}$ ,  $\mathcal{F}_{rj}$ , and  $\mathcal{P}_{rj}$  as is discussed in section 2.2.1. These variables are used in jet equation.

Step 3: The extra compression in the post-shock flow drives bipolar outflows, and the entire post-shock disc participates in jet generation (Molteni *et al.* 1994, 1996a; Nagakura & Yamada 2009; Nishikawa *et al.* 2005). The jet base is the post-shock disc, so the jet is launched with the post-shock disc quantities. If  $x = x_b$  is the jet launch site in the post-shock disc, then the specific energy of the disc at  $x_b$  *i.e.*,  $\mathcal{E}_b = \mathcal{E}(x_b)$ , and the post-shock specific angular momentum at  $x_b$  *i.e.*,  $\lambda_b = \lambda(x_b)$  and the



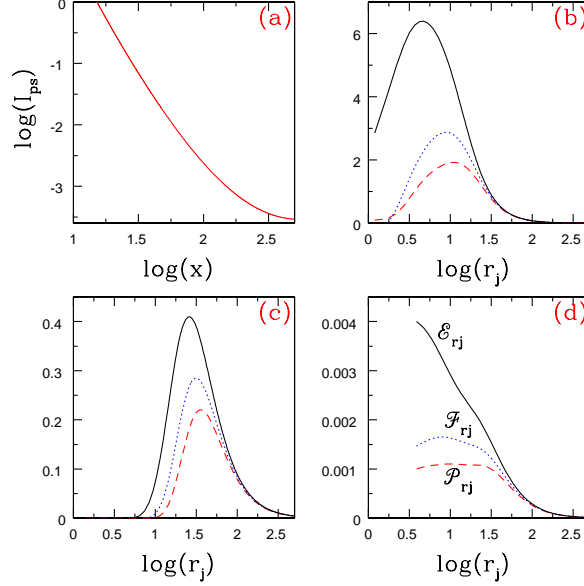


**Figure 2.** (a) Normalized intensity of synchrotron radiations (solid line, online red) from pre-shock disc with  $\log(x)$  (b) Moments of the radiation field due to the post-shock disc  $\mathcal{E}_{r_j s}/\mathcal{K}_0$  (solid, online black),  $\mathcal{F}_{r_j s}/\mathcal{K}_0$  (dotted, online blue) and  $\mathcal{P}_{r_j s}/\mathcal{K}_0$  (dashed, online red), are plotted with  $\log(r_j)$ , and (c)  $\mathcal{E}_{r_j ps}/\mathcal{J}_0$  (solid, online black),  $\mathcal{F}_{r_j ps}/\mathcal{J}_0$  (dotted, online blue) and  $\mathcal{P}_{r_j ps}/\mathcal{J}_0$  (dashed, online red), the moments of the radiation field due to the pre-shock disc are plotted. (d) Total moments of radiation field due to post-shock and pre-shock disc, are generated by an accretion disc with parameters  $E = 3.5 \times 10^{-3}$ ,  $\lambda_0 = 1.5435$ ,  $\alpha = 0.02$ ,  $\gamma = 1.4$  (forming shock at  $x_s = 15.18$ ). The radiation field is for equal post-shock and pre-shock luminosities  $\ell_s = \ell_{ps} = 0.4$ .

density at the top of the disc at  $x_b$  *i.e.*,  $\rho_b$ , are the flow variables of the jet at its base. Here we have taken  $x_b = (x_{ci} + x_s)/3$ , and since the disc is assumed to be in hydrostatic equilibrium along the  $z$  direction,  $\rho_b = \rho(x_b)\exp(-2y_b/h_s)$ , where,  $y_b$  is the height of the disc at  $x_b$ , and  $h_s$  is disc height at shock location. The jet velocity  $v_{jb}$  and the sound speed  $a_{jb}$  at the jet base are not arbitrarily assigned, but are computed self consistently. We eliminate  $a_j$  from Eq. (12) and Eq. (10), and express  $\mathcal{E}_b$  in terms of  $\dot{\mathcal{M}}_j$ ,  $v_{jb}$ ,  $\lambda_b$  etc. Since  $\mathcal{E}_b$  and  $\lambda_b$  are obtained from the post-shock disc and therefore known for the jet, we iterate with various values of entropy *i.e.*,  $\dot{\mathcal{M}}_j$  to obtain the correct value of  $v_{jb}$  and  $a_{jb}$ , with which the unique transonic solution is determined by integrating Eq. (13) and checking for the sonic point conditions Eqs. (16,17). Once the transonic jet solution is obtained, then  $R_{\dot{m}}$  is easily calculated from Eq. (22).

Step 4: Now the information of  $R_{\dot{m}}$  is used in the shock condition (Eqs. 20 - 22) and then go back to Step 1 to recalculate the new accretion solution, the new radiative moments (Step 2), and the new jet solution (Step 3). This process is repeated till the shock location converges to a value ( $x_s$ ), and we find out the self-consistent, converged accretion-ejection solution.

Therefore, there are three iteration processes, namely, (1) to find out inner sonic point of accretion disc, (2) accretion shock and the outer sonic point, and (3) the jet sonic point when launched with the post-shock disc variables.

### 2.2.1 Radiative moments

Now as the jet is generated due to compression as well as shock heating from the post-shock disc (see Fig. 1), the jet will be moving through the radiation field of the accretion disc. We now outline the method to compute radiative moments and the net radiative acceleration of the jet. The radiative acceleration term is proportional to the radiative flux  $F_{r_j}$ , but the radiation drag term (negative terms in r. h. s of Eq. 9) depends on jet flow velocity  $v_j$ , the radiation energy density  $\mathcal{E}_{r_j}$  and the radiation pressure  $\mathcal{P}_{r_j}$ . Figure 1 shows the schematic diagram of the radiations coming from various parts of the disc, and how it can interact with the outflowing jet, generated due to shock heating of the inner disc. The radiative moments along the jet streamlines ( $r_j$ ) are calculated from the post-shock ( $s$ ) and pre-shock ( $ps$ ) disc respectively. The radiative terms in Eq. 9 are given by,

$$\mathcal{E}_{r_j} = \frac{\sigma_T}{mc} \left( \int I_s d\Omega_s + \int I_{ps} d\Omega_{ps} \right) = \frac{\sigma_T}{m} (E_{r_j s} + E_{r_j ps}) = \mathcal{E}_{r_j s} + \mathcal{E}_{r_j ps} \quad (23)$$

$$\mathcal{F}_{r_j} = \frac{\sigma_T}{mc} \left( \int I_s r_j d\Omega_s + \int I_{ps} r_j d\Omega_{ps} \right) = \frac{\sigma_T}{mc} (F_{r_j s} + F_{r_j ps}) = \mathcal{F}_{r_j s} + \mathcal{F}_{r_j ps} \quad (24)$$

$$\mathcal{P}_{r_j} = \frac{\sigma_T}{mc} \left( \int I_s \hat{r}_j \hat{r}_j d\Omega_s + \int I_{ps} \hat{r}_j \hat{r}_j d\Omega_{ps} \right) = \frac{\sigma_T}{m} (P_{r_{js}} + P_{r_{jps}}) = \mathcal{P}_{r_{js}} + \mathcal{P}_{r_{jps}} \quad (25)$$

Since the jet streamline is close to the axis of symmetry, we calculate the radiative moments on the axis and approximate these to hold at the same radial distance on the jet streamline. In this paper, we are not dealing with the detailed features of the radiation spectrum from the accretion disc. Rather, we are interested to see the effect of the total pre-shock and post-shock radiation on the acceleration of the jet. Hence, we do not include radiative transfer dynamically into the hydrodynamic solution. To calculate the moments of radiation due to the pre-shock disc, as an example, we consider only synchrotron processes from the pre-shock disc.

The synchrotron emissivity is due to the presence of stochastic magnetic field, where the magnetic pressure ( $p_m$ ) is in partial equipartition with the gas pressure ( $p_g$ ), *i.e.*,

$$p_m = \frac{B^2}{8\pi} = \beta p_g; \quad \text{where, } 0 \leq \beta \leq 1,$$

here, for  $\beta = 0$  implies no magnetic field and therefore the total pressure in Eq. (1)  $p = p_g$ , while  $\beta = 1$  implies strict equipartition between gas and magnetic pressure and therefore  $p = p_g + p_m$ . The analytical expression for synchrotron emissivity is given by (Shapiro & Teukolsky 1983), and the resulting intensity is,

$$I_{ps} = I_{syn} = \frac{16}{3} \frac{e^2}{c} \left( \frac{eB}{m_e c} \right)^2 \Theta^2 n_e \left( \frac{hr_g}{\sec\theta_{ps}} \right) \text{ erg cm}^{-2} \text{ s}^{-1} \quad (26)$$

where,  $\Theta, n_e, h$  and  $\theta_{ps}$  are the pre-shock local dimensionless temperature  $k_b T / (m_e c^2)$ , electron number density, disc half height and angle from the axis of symmetry to the pre-shock disc surface, respectively. The dependence of  $I_{ps}$  on disc radius is through flow variable like  $T$  &  $n_e$ . Integrating  $I_{ps}$  over the pre-shock disc gives us the pre-shock luminosity  $\ell_{ps}$ . The radiative intensity from the post shock disc is  $I_s = \ell_s / A_s$ , where  $\ell_s$  is the post-shock luminosity in units of Eddington luminosity and  $A_s$  is the total surface area of the post-shock disc. The total luminosity is  $\ell = \ell_s + \ell_{ps}$ . The moments of the radiation field above the accretion disc was calculated before (Chattopadhyay & Chakrabarti 2000, 2002; Chattopadhyay *et al.* 2004; Chattopadhyay 2005), and for the above mentioned approximations, they are given by,

$$\mathcal{E}_{r_{js}} = 2\pi \mathcal{K}_0 \int_{x_{in}}^{x_s} \frac{zxdx}{[(z-x \cot\theta_s)^2 + x^2]^{3/2}}; \quad \mathcal{E}_{r_{jps}} = 2\pi \mathcal{J}_0 \int_{x_s}^{x_{inj}} \frac{a^5 zxdx}{u^2 x^{3/2} (x-1) [(z-x \cot\theta_{ps})^2 + x^2]^{3/2}}, \quad (27)$$

$$\mathcal{F}_{r_{js}} = 2\pi \mathcal{K}_0 \int_{x_{in}}^{x_s} \frac{z(z-x \cot\theta_s)xdx}{[(z-x \cot\theta_s)^2 + x^2]^2}; \quad \mathcal{F}_{r_{jps}} = 2\pi \mathcal{J}_0 \int_{x_s}^{x_{inj}} \frac{a^5 z(z-x \cot\theta_{ps})xdx}{u^2 x^{3/2} (x-1) [(z-x \cot\theta_{ps})^2 + x^2]^2}, \quad (28)$$

$$\mathcal{P}_{r_{js}} = 2\pi \mathcal{K}_0 \int_{x_{in}}^{x_s} \frac{z(z-x \cot\theta_s)^2xdx}{[(z-x \cot\theta_s)^2 + x^2]^{5/2}}; \quad \mathcal{P}_{r_{jps}} = 2\pi \mathcal{J}_0 \int_{x_s}^{x_{inj}} \frac{a^5 z(z-x \cot\theta_{ps})^2xdx}{u^2 x^{3/2} (x-1) [(z-x \cot\theta_{ps})^2 + x^2]^{5/2}}, \quad (29)$$

where,  $\theta_s = \tan^{-1}(x_s/h_s)$ ,  $h_s = \sqrt{(2/\gamma)a_s + x_s^{1/2}}(x_s - 1)$  and  $\theta_{ps} = \tan^{-1}(x/h)$  for pre-shock disc, *i.e.*, for  $x > x_s$ . Moreover,

$$\mathcal{K}_0 = \frac{1.3 \times 10^{38} \ell_s \sigma_T}{2\pi c m_p A_s G M_\odot} \quad (30)$$

$$\text{and, } \mathcal{J}_0 = \frac{2.93 \times 10^{34} e^4 \mu^2 \beta \sigma_T \dot{m}^2}{3\pi m_e^4 c^2 \sec\theta_{ps} \gamma^{5/2} G^2 M_\odot^2} \quad (31)$$

where,  $\dot{m}$  is the accretion rate in units of Eddington accretion rate,  $\sigma_T$  is Thomson scattering cross section,  $\mu$  is mean molecular weight of the plasma,  $m_p$  is the proton mass,  $m_e$  is the electron mass and  $M_\odot$  is the solar mass. It is to be noted that the pre-shock radiation would depend on the product  $\beta \dot{m}^2$ . It is interesting to know that, the post-shock region by virtue of its geometry will block some of the pre-shock photons to the base of the jet, an effect coined as the shadow effect of the post-shock disc (Chattopadhyay *et al.* 2004; Chattopadhyay 2005). That is to say, if the height of the jet is  $y_j < y_{jl}$ , then  $\mathcal{E}_{r_{jps}} = \mathcal{F}_{r_{jps}} = \mathcal{P}_{r_{jps}} = 0$ , where

$$y_{jl} = h_s - \frac{h_{inj} - h_s}{x_{inj} - x_s} (x_s - x_j), \quad (32)$$

here,  $h_{inj}$  &  $x_{inj}$  are height and radius at outer edge of the disc. Additionally due to the shadow effect, the inner edge of the pre-shock disc as seen by an observer at some height  $y_j$  will be,

$$x_i = -\frac{x_s y_j}{h_s - y_j - x_s \cot\theta_{ps}}$$

In this paper, we use  $\beta \dot{m}^2$  as a supplied parameter to calculate  $\ell_{ps}$ . Also we use  $\ell_s$  initially as a parameter (except Fig. 8 and Fig. 9) in order to understand the effect of the relative proportions of radiation coming from different parts of disc on the ejected jet, but finally we will use the relation  $\ell_s / \ell_{ps}$  as a function of  $x_s$  (see Appendix), to compute  $\ell_s$  from the pre-shock radiation, and solve the accretion-ejection solution.

In Figs. 2a-d, all the plots are generated for a disc characterized by  $(E, \lambda_0, \alpha, \gamma) = (3.5 \times 10^{-3}, 1.5435, 0.02, 1.4)$ , which generates a shock at  $x_s = 15.18$ . In Fig. 2a,  $I_{ps}$  is plotted as a function of  $x$ , starting from  $x_s$  outwards. In Fig. 2b, we plot



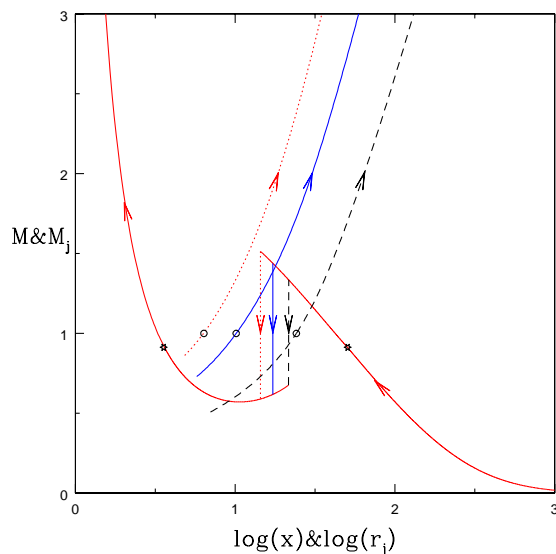


**Figure 3.** Accretion Mach number ( $M$ ) and jet Mach number ( $M_j$ ) with radial distance  $x$  and jet streamline  $r_j$  in log scale, are shown in the plot. Open circle represents the critical points of jets and star marks for accretion solutions, while arrows show flow directions. Solid curve (red online) with inward arrows is accretion solution for parameters  $E = 3.3 \times 10^{-3}$ ,  $\lambda_0 = 1.353$ ,  $\alpha = 0.1$ . The post shock disc generate jets. Each jet curve represents  $M_j$  vs  $\log(r_j)$  for parameters  $\ell_s = 0.0$  ( $\ell = 0.0386$ ) (dashed, online black),  $\ell_s = 0.1$  ( $\ell = 0.151$ ) (solid, online blue), and  $\ell_s = 0.2$  ( $\ell = 0.274$ ) (dotted, online red). The shocks are shown by vertical jumps (line style and color corresponds to that of the jet it generates). The parameter  $\beta\dot{m}^2 = 0.01$  is kept constant.

$\mathcal{E}_{r_{js}}/\mathcal{K}_0$  (solid, online black),  $\mathcal{F}_{r_{js}}/\mathcal{K}_0$  (dotted, online blue) and  $\mathcal{P}_{r_{js}}/\mathcal{K}_0$  (dashed, online red), the radiation moments due to the post-shock disc. In Fig. 2c, we plot  $\mathcal{E}_{r_{jps}}/\mathcal{J}_0$  (solid, online black),  $\mathcal{F}_{r_{jps}}/\mathcal{J}_0$  (dotted, online blue) and  $\mathcal{P}_{r_{jps}}/\mathcal{J}_0$  (dashed, online red), the radiation moments due to the pre-shock disc. The shadow effect of the post-shock disc is clearly shown in the figure. In Fig. 2d, we plot  $\mathcal{E}_{r_j}$  (solid, online black),  $\mathcal{F}_{r_j}$  (dotted, online blue) and  $\mathcal{P}_{r_j}$  (dashed, online red) taking equal post-shock and pre-shock luminosities,  $\ell_s = \ell_{ps} = 0.4$ , respectively. From the above figures it is clear that radiative moments from the post shock region peaks at a height closer to the black hole and the moments from the pre-shock disc peaks typically at a distance few times larger. However, the space dependent parts of the moments (Figs. 2b-c) shows that the moments of radiation from the pre-shock disc is typically an order of magnitude weaker than those due to the post-shock disc. However, the second distinct bulge in Fig. 2d shows, if the pre-shock luminosity is comparable to post-shock luminosity then the radiation moments peaks at two places, and hence presents a prospect for multi-stage acceleration scheme for the jets.

### 3 RESULTS

In Kumar & Chattopadhyay (2013) we have shown in details various cases of accretion solutions, and also have shown that post shock disc naturally produces bipolar outflows. In this paper, therefore we discuss only the shocked accretion solution. The accretion solutions are characteristic by flow parameters like the grand energy  $E$ , the specific angular momentum at the horizon  $\lambda_0$  (conversely,  $\lambda_{in_j}$  at the outer edge of the disc) and the viscosity parameter  $\alpha$ . The jet is launched from the disc with the specific energy ( $\mathcal{E}_j$  and angular momentum ( $\lambda_j$ ) of the post-shock disc at the jet launch site ( $r_b$ ). We also compute the moments of radiation fields ( $\mathcal{E}_{r_j}$ ,  $\mathcal{F}_{r_j}$ ,  $\mathcal{P}_{r_j}$ ) above the disc, and are used to accelerate the jets. The pre-shock disc radiation depends on  $\beta\dot{m}^2$ , where,  $\beta$  is the ratio of the magnetic and the gas pressure and  $\dot{m}$  is the accretion rate in units of Eddington rate. In order to find the effect of post-shock radiation and pre-shock radiation on jet acceleration, the post-shock luminosity  $\ell_s$  and  $\beta\dot{m}^2$  (conversely,  $\ell_{ps}$  the pre-shock luminosity) are supplied as independent parameters. However, since post-shock radiation is produced by inverse-Comptonization of self generated and intercepted photons from the pre-shock disc, we compute the post-shock radiation self-consistently by employing the techniques of Chakrabarti & Mandal (2006). And in Figs. (8, 9, 10) the jets are accelerated by self consistent estimation of radiation field, both from pre and post-shock discs.

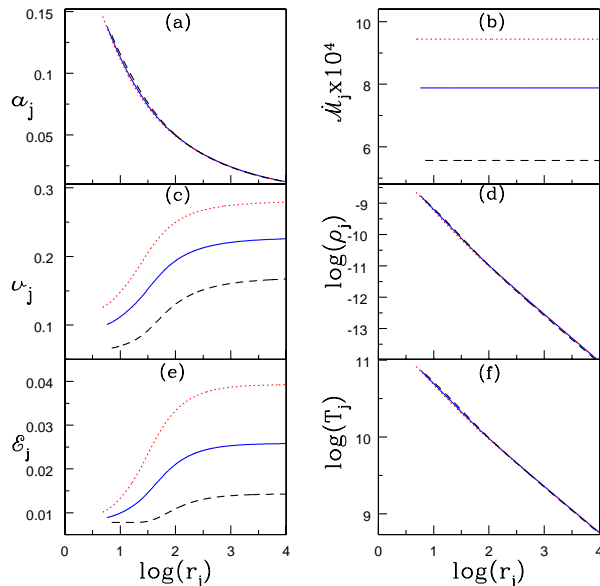


**Figure 4.** Jet flow variables like (a) sound speed  $a_j$ , (b) entropy-accretion rate  $\dot{M}_j$ , (c) jet velocity  $v_j$ , (d) density  $\rho_j$ , (e) specific energy  $\mathcal{E}_j$ , and (f) temperature  $T_j$  are plotted with  $\log(r_j)$ . The disc, radiation parameters, the line colours and line styles are same as Fig. 3.

### 3.1 Effect of post-shock radiation on jet acceleration

The radiations produced from accretion is governed by the solution. However, we will now treat the post-shock luminosity as a parameter just to see how it affects the jet acceleration. The accretion Mach number  $M = u/a$  with  $\log(x)$  is plotted for the parameters  $E = 3.3 \times 10^{-3}$ ,  $\lambda_0 = 1.353$ ,  $\alpha = 0.1$ , in Fig. 3. We first consider  $\ell_s = 0$  and  $\beta \dot{m}^2 = 0.01$ , the shock is at  $x_s = 21.546$  (vertical dashed, online black), and drives bipolar outflow, where the jet Mach number  $M_j$  (dashed, online black) is plotted with  $\log(r_j)$ , and the mass outflow rate is  $R_{\dot{m}} = 0.032$  and the sonic point of the jet is at  $r_{jc} = 24.160$ . Radiation field from the accretion disc deposit its momentum and accelerate the shock generated jets. Assuming  $\ell_s = 0.1$  for same set of accretion boundary condition, accretion-ejection solution is computed. The shock is found to be at  $x_s = 17.92$  (solid, online blue) and the jet  $M_j$  distribution (solid, online blue) has a sonic point at  $r_{jc} = 9.59$  and  $R_{\dot{m}} = 0.046$ . The total luminosity for this case is  $\ell = (\ell_s + \ell_{ps}) = 0.151$  ( $\ell_s = 0.1$ ). Keeping  $\beta \dot{m}^2$  same, we increase  $\ell_s = 0.2$ , so the total luminosity increases to  $\ell = 0.274$ . The accretion-ejection solution shows that the mass outflow increases to  $R_{\dot{m}} = 0.058$  and the shock in accretion decreases to  $x_s = 14.4$  (dotted, online red). In this case too, due to the increase of radiation, the sonic point decreases to  $r_{jc} = 6.36$ , indicating stronger jet. It is interesting to note that, the pre-shock luminosity increases even though  $\beta \dot{m}^2$  is kept constant, because, with the decrease in  $x_s$ , the size of the pre-shock disc increases.

The jet solutions are explored in more details in the following figure. Jet variables  $a_j$  (Fig. 4a),  $\dot{M}_j$  (Fig. 4b),  $v_j$  (Fig. 4c),  $\rho_j$  (Fig. 4d),  $\mathcal{E}_j$  (Fig. 4e) and  $T_j$  (Fig. 4f) are plotted with  $\log(r_j)$ . Each curve corresponds to  $\ell_s = 0$  (dashed, online black),  $\ell_s = 0.1$  (solid, online blue), and  $\ell_s = 0.2$  (dotted, online red), and which are exactly the same cases of jet solutions as in Fig. 3. The increase in  $\ell_s$ , accelerates the jets further, and therefore increases  $R_{\dot{m}}$ , this in turn decreases the post-shock pressure and the location of the shock front moves close to the horizon. As a result the jet base moves closer. At a given  $r_j$ , we find  $v_j$  is higher for higher  $\ell_s$ , but difference in  $a_j$  or  $T_j$  are imperceptible. This shows, that enhanced jet acceleration is due to the radiative momentum deposition onto the jets and not due to conversion of thermal energy to the kinetic one. Since higher  $\ell_s$  accelerate the jet, the sonic point is formed closer to the horizon. Higher  $\ell_s$  not only means faster jet, but also a jet with higher entropy (Fig. 4b).

The jet terminal speed is defined as  $v_\infty = v$  (at  $r_j \rightarrow \text{large}$ ) where  $dv_j/dr_j \rightarrow 0$ . As shown in Figs. 4,  $v_\infty$  increases appreciably with the increase of  $\ell_s$  and  $\ell_{ps}$ , for a given value of disc viscosity parameter  $\alpha$ . We would like to see whether this behaviour of  $v_\infty$  holds true for a range of  $\alpha$ . In Fig. 5a,  $v_\infty$  is plotted with  $\ell_s$ , in Figs. 5b & 5f,  $v_\infty$  is plotted with  $x_s$  and the jet base specific energy  $\mathcal{E}_b$ . And  $R_{\dot{m}}$  is plotted with  $\ell_s$  (Fig. 5c) and  $x_s$  (Fig. 5d). Each curve correspond for  $\alpha = 0.04944$  (solid, online red),  $0.049887$  (dotted, online blue), and  $0.050113$  (dashed, online black). All these figures are generated with outer boundary condition  $E = 0.001$  and  $\lambda_{inj} = 70.6$  at  $x_{inj} = 10^4$ . It is clear that  $v_\infty$  increases with  $\ell_s$  at a given value of  $\alpha$ , as well as, increases with  $\alpha$  at a given  $\ell_s$ . Since  $x_s$  moves closer with the increase of both  $\ell_s$  and  $\alpha$ , the jets are launched with higher  $\mathcal{E}_b$ , which in turn increases  $v_{jb}$ . This is also the reason that the relative mass outflow rate  $R_{\dot{m}}$  increases with the increase of both  $\ell_s$  and  $\alpha$ . Since  $v_{jb}$  increases with  $\ell_s$  and  $\alpha$ , therefore the jets become supersonic at a distance nearer to the jet base, *i.e.*,  $r_{jc}$  decreases with the increase of  $\ell_s$  (Fig. 5e).

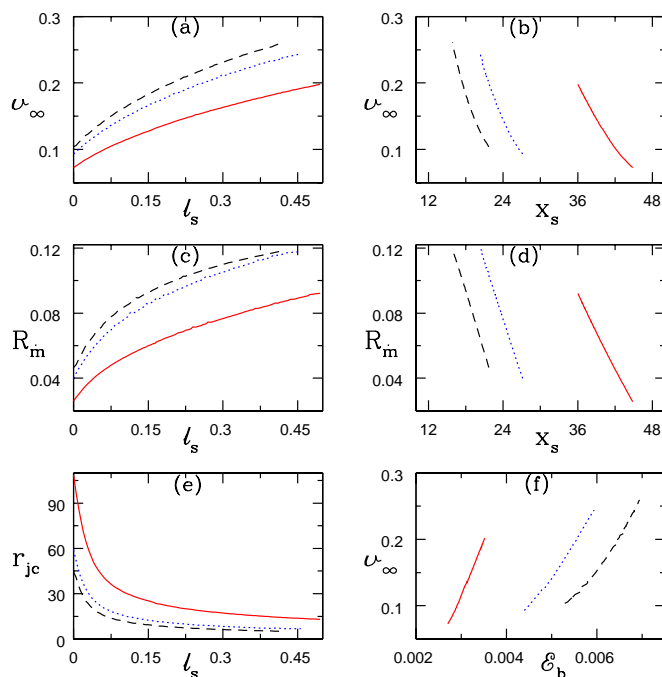


**Figure 5.** Jet terminal velocity  $v_\infty$  is plotted with  $\ell_s$  (a), with  $x_s$  (b), and with  $\mathcal{E}_b$  (f).  $R_{\dot{m}}$  is plotted with  $\ell_s$  (c) and  $x_s$  (d). Moreover,  $r_{jc}$  is plotted with  $\ell_s$  (e) too. The accretion solution corresponds to disc parameters  $E = 0.001$  and  $\lambda_{inj} = 70.6$  at disc outer boundary  $x_{inj} = 10^4$  and keeping pre-shock luminosity is  $\ell_{ps} = 0.0$ . Each curve correspond for  $\alpha = 0.04944$  (solid, online red),  $0.049887$  (dotted, online blue), and  $0.050113$  (dashed, online black).

### 3.2 Effect of pre-shock radiation on jets

The effect of radiation from pre-shock disc as it impinges on the jet is illustrated through Figs. 6b-f. In Fig. 6a, the Mach number  $M$  of the accretion solution is plotted with  $\log(x)$  for disc parameters  $E = 3.3 \times 10^{-3}$ ,  $\lambda_0 = 1.353$ , and  $\alpha = 0.1$ . The shock is at  $x_s = 17.92$ . We choose  $\ell_s = 0.1$ , but the pre-shock radiation is changed by varying  $\beta\dot{m}^2$ . The solutions correspond to  $\beta\dot{m}^2 = 0.01$  ( $\ell = 0.151$ ) (solid, online red),  $\beta\dot{m}^2 = 0.02$  ( $\ell = 0.202$ ) (dotted, online blue), and  $\beta\dot{m}^2 = 0.04$  ( $\ell = 0.303$ ) (dashed, online black). The post-shock disc actually hides the base of the jet from most of the radiation from the pre-shock disc, while shines its own light onto the jets (see Fig. 1). As a result, if the post-shock radiation remains unaltered and the jet sonic point is formed in the portion of the funnel like region where pre-shock radiation is negligible, then the jet base velocity  $v_{jb}$ , the jet base  $r_{jb}$  or the jet base properties are likely to remain roughly same, keeping the massloss rate unaltered. Consequently, the change in the accretion shock is imperceptible (Fig. 6a). All the jet variables closer to the base, *e.g.*,  $M_j$  (Fig. 6b),  $v_j$  (Fig. 6c),  $\mathcal{E}_j$  (Fig. 6e), and  $T_j$  are indistinguishable, while they differ from each other in the supersonic region, where the interaction of pre-shock radiation with the jet is significant too. It is to be remembered, that the temperature plotted here is the single temperature of the outflow. The corresponding electron temperature should be about 2 orders of magnitude less. However, the entropy accretion rates  $\dot{\mathcal{M}}$  (Fig. 6d) are distinguishable even at the base. Once again it is clear from the temperature plot, that radiative driving is significant. It is also interesting to note from Figs. 3-4, that increasing  $\ell_s$ , would result in faster jets, with higher  $R_{\dot{m}}$  and lower jet sonic point ( $r_{jc}$ ). While increasing the pre-shock radiation also results in faster jets, but with almost no change in  $R_{\dot{m}}$  and  $r_{jc}$ . Since relative mass outflow rates affects the accretion solutions (Eq. 22), so the feed-back effect of the jet on the disc due to  $\ell_s$  might be more significant than that due to  $\ell_{ps}$ .

In Figs. 7a-d, we investigate how  $\ell_{ps}$  affects the jet solutions for a variety of  $\alpha$ , but for the same outer boundary condition as in Fig. 6 with constant  $\ell_s = 0.2$ . In Fig. 7a, we plot  $v_\infty$  as a function of  $\ell$ , where each curve represent disc solutions with  $\alpha = 0.04944$  (solid, online red),  $0.049887$  (dotted, online blue), and  $0.050113$  (dashed, online black). In all these plots  $\ell_{ps}$  varies from  $0 \rightarrow 0.6$ . Due to radiative driving,  $v_\infty$  increases with  $\ell$ , and at a given  $\ell$ , it increases with  $\alpha$ . As has been explained in connection to the previous figure, increasing  $\alpha$  for a fixed outer boundary decreases  $x_s$ , which means the jet base energy  $\mathcal{E}_b$  increases, resulting in faster jet. However, since the pre-shock disc primarily shines the radiation on the supersonic part of the jet, therefore  $\ell_{ps}$  has marginal effect on  $r_{jc}$ , and  $v_{jb}$ . Therefore,  $R_{\dot{m}}$  is almost constant with the change of  $\ell_{ps}$  (Fig. 7d), which in turn keeps  $x_s$  almost unchanged (Fig. 7b), and the jet sonic point  $r_{jc}$  also remains unchanged (Fig. 7c). In other words, we may conclude, that the radiation from the inner torus of the accretion disc accelerate the jet, but also increases net mass-loss. On the other hand, radiation from pre-shock disc or the outer disc, accelerates the jet appreciably, although, has almost no

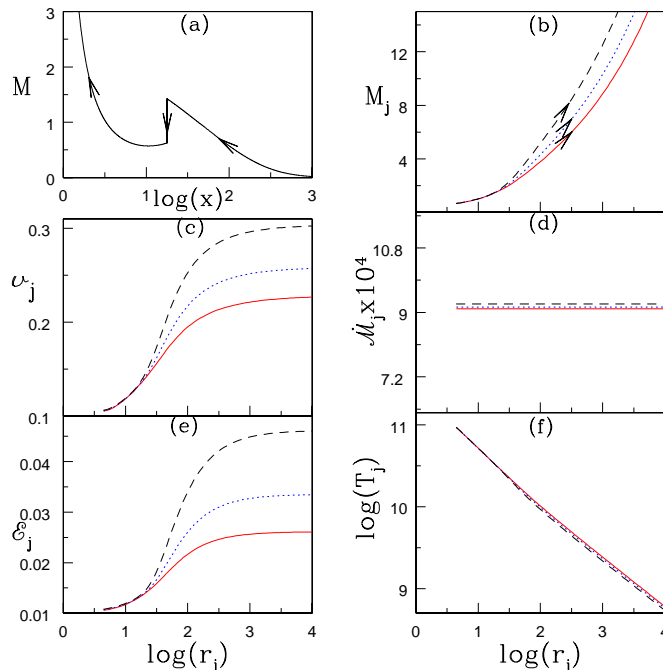


**Figure 6.** (a) Accretion Mach Number  $M$  with  $\log(x)$ , and (b) jet Mach number  $M_j$ , (c) jet velocity  $v_j$ , (d) jet entropy rate  $\dot{M}_j$ , (e) specific energy  $\mathcal{E}_j$ , and (f) temperature  $T_j$  plotted with  $\log(r_j)$  for the disc parameters  $E = 3.3 \times 10^{-3}$ ,  $\lambda_0 = 1.353$ ,  $\alpha = 0.1$ , and shock forms at  $x_s = 17.92$ . Each curve is for  $\beta \dot{m}^2 = 0.01$  ( $\ell = 0.151$ ) (solid, online red),  $\beta \dot{m}^2 = 0.02$  ( $\ell = 0.202$ ) (dotted, online blue), and  $\beta \dot{m}^2 = 0.04$  ( $\ell = 0.303$ ) (dashed, online black) and  $\ell_s = 0.1$  is kept constant. Each jet solutions have critical points at  $r_{jc} \sim 9.59$  and mass outflow rates,  $R_{\dot{m}} \sim 0.046$ .

effect on  $R_{\dot{m}}$ . Therefore, in the second case we may obtain jets with higher kinetic luminosity. This conclusion is valid for any value of  $\alpha$  which admits accretion shock.

### 3.3 Radiative driving of jets with computed post-shock and pre-shock radiations

Having investigated the role the pre-shock and post-shock radiation may have on jets, we actually calculate the  $\ell_s$  from  $\ell_{ps}$ . In appendix A, we have discussed the different radiation processes in a general radiative transfer model (Chakrabarti & Mandal 2006). From the accretion disc spectrum, we calculate the ratio of post-shock to pre-shock luminosity ( $\ell_s/\ell_{ps}$ ) using the viscous transonic solution. We then use a fitting formula of  $\ell_s/\ell_{ps}$  (Eq. A1) to calculate the ratio at any given shock location ( $x_s$ ). In (Fig. A1b), a typical  $\ell_s/\ell_{ps}$  dependence on  $x_s$  is obtained where the dots are the data points from model (Chakrabarti & Mandal 2006) and solid line represents the fitting function. We assume that the behaviour of this ratio with shock location is generic. The procedure for calculating  $\ell_s$  is as follows — for a given set of values of  $E$ ,  $\lambda_0$ ,  $\alpha$ , the accretion solution shows a shock at  $x_s$  and a bipolar outflow with some  $R_{\dot{m}}$ . We then calculate  $\ell_{ps}$  (Eq. 26) by supplying  $\beta \dot{m}^2$  and the density and temperature distribution between  $x_{inj}$  and  $x_s$ . We use the fitting formula of  $\ell_s/\ell_{ps}$  (Eq. A1) to calculate  $\ell_s$ . Using these the jet solution is obtained. All the solutions presented in Figs. (3-7), we have solved the accretion ejection solution with the following fluid parameters  $E$ ,  $\lambda_0$  (at the horizon, or equivalently,  $\lambda_{inj}$  at the outer boundary),  $\alpha$ , and in addition the radiation parameters  $\ell_s$  and  $\beta \dot{m}^2$  (equivalently  $\ell_{ps}$ ). Now, following the procedures described in appendix A, we reduce one parameter, namely,  $\ell_s$ . In Fig. 8a, we plot  $x_s$  with  $\lambda_0$ , in fig. 8b, we plot the compression ratio  $R$  with  $x_s$ , and in fig. 8c, mass outflow rate  $R_{\dot{m}}$  with the compression ratio  $R$ . All the plots are for accretion disc parameters  $E = 0.004$ ,  $\alpha = 0.01$ , and various results has been obtained by varying  $\lambda_0$ . The curves are for thermally driven jet (*i.e.*,  $\beta \dot{m}^2 = 0$ ; dashed, online red), and thermal plus radiatively driven jets (*i.e.*,  $\beta \dot{m}^2 = 0.005$ ; dotted online blue, and  $\beta \dot{m}^2 = 0.01$ ; solid, online black). This shows that as the compression at the shock increases, it forces more matter into the jet channel. Although  $R$  increases as  $x_s$  decreases, but smaller post-shock region means less matter can be driven as jets, so  $R_{\dot{m}}$  maximizes at some intermediate  $R$ . It has also been shown earlier (Chakrabarti 1999; Das *et al.* 2001), that for  $R = 1$  *i.e.*, no shock,  $R_{\dot{m}} \sim 0$  *i.e.*, for no shock there is no outflow.

In Figs. 9a-l, we have plotted accretion and jet solutions for various  $\alpha$  and  $\ell_{ps}$ . All the accretion solutions ( $M$  with  $\log(x)$ ) are for outer boundary parameters  $E$ ,  $\lambda_{inj} = 0.001$ , 18.592 at the outer boundary  $x_{inj} = 10^4$ . The viscosity parameters are  $\alpha = 9.115 \times 10^{-3}$  (9a),  $9.315 \times 10^{-3}$  (9d),  $9.626 \times 10^{-3}$  (9g), and  $9.875 \times 10^{-3}$  (9j). The vertical jumps show the location of accretion shocks, and they are at  $x_s = 125.896$  (9a), 45.9986 (9d), 18.2871 (9g), and 8.5741 (9j). The jet

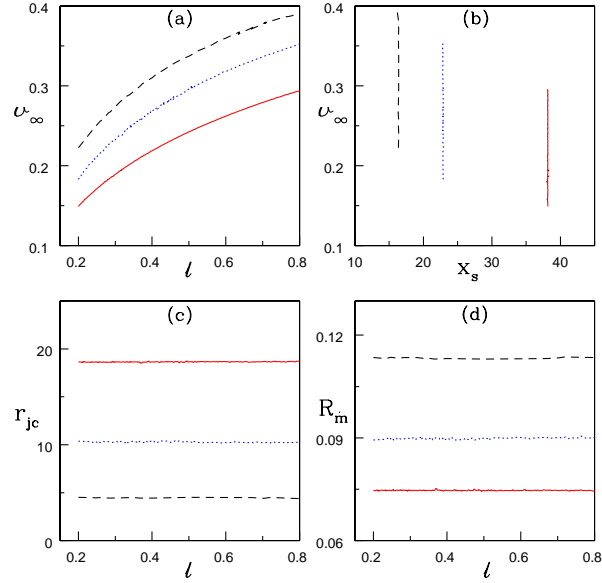


**Figure 7.** Terminal jet velocity  $v_\infty$  with total disc luminosity  $\ell$ , (b) shock locations  $x_s$ , and (c)  $r_{jc}$  is plotted with  $\ell$  and (d)  $R_m$  is plotted with  $\ell$ . The disc parameters are  $E = 0.001$  and  $\lambda_{inj} = 70.6$  at disc outer boundary  $x_{inj} = 10^4$ , and keeping post-shock luminosity is  $\ell_s = 0.2$  but varying pre-shock luminosity ( $\ell_{ps}$ ). Each curve are for viscosity parameter  $\alpha = 0.04944$  (solid, online red),  $0.049887$  (dotted, online blue), and  $0.050113$  (dashed, online black).

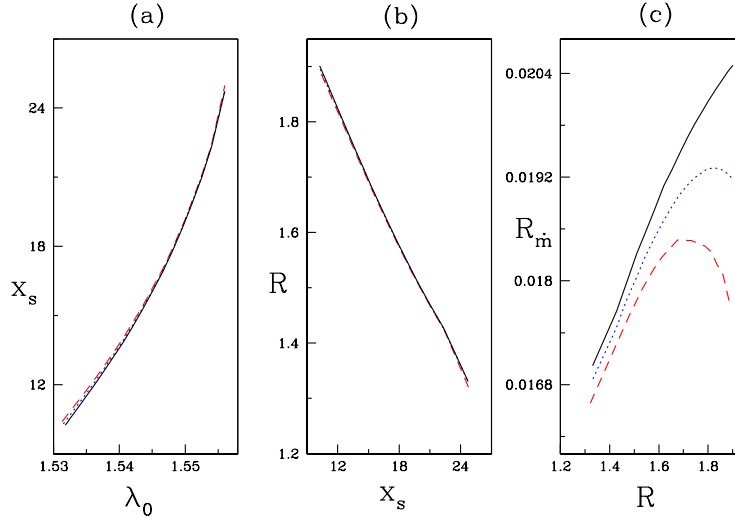


**Figure 8.** (a) Shock location  $x_s$  is plotted with angular momentum at the horizon ( $\lambda_0$ ), (b) Compression ratio  $R$  with  $x_s$  and (c) mass outflow rate ( $R_m$ ) versus  $R$  are plotted for flows with  $E = 0.004$ ,  $\alpha = 0.01$ . Various plots represent thermally driven flow (dashed, online red), and radiatively driven outflows for  $\beta\dot{m}^2 = 0.005$  (dotted, online blue) and  $\beta\dot{m}^2 = 0.01$  (solid, online black).

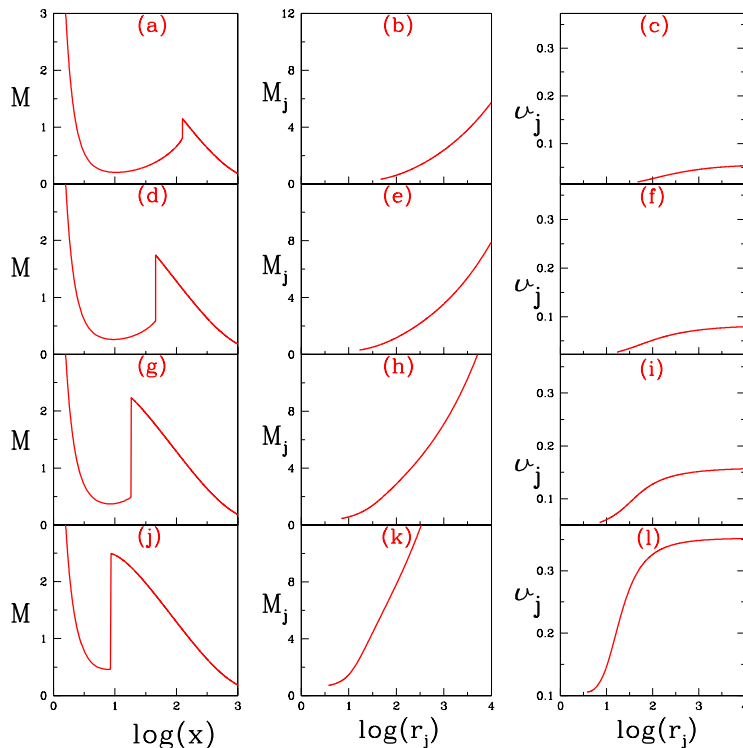


**Figure 9.** Variations of accretion Mach number  $M$  (a, d, g, and j) with  $\log(x)$ ,  $M_j$  (b, e, h, and k), and  $v_j$  (c, f, i, and l) with  $\log(r_j)$ . The disc solutions are for parameters  $E = 0.001$ ,  $\lambda_{inj} = 18.592$  at outer boundary  $x_{inj} = 10^4$ , and for  $\alpha = 0.009115$  (a-c), 0.009315 (d-f), 0.009626 (g-i), and 0.009875 (j-l). Plots (a-c) are characterized by  $(x_s, R_{\dot{m}}, \ell_{ps}, \ell_s = 125.8964, 0.0091, 0.0054, 0.0346)$ ; for (d-f)  $(x_s, R_{\dot{m}}, \ell_{ps}, \ell_s = 45.9986, 0.0208, 0.0103, 0.0438)$ ; for (g-i)  $(x_s, R_{\dot{m}}, \ell_{ps}, \ell_s = 18.2871, 0.0504, 0.0380, 0.0585)$ ; and for (j-l)  $(x_s, R_{\dot{m}}, \ell_{ps}, \ell_s = 8.5741, 0.0991, 0.2337, 0.0948)$ , and the jet terminal velocities are  $v_\infty = 0.0534, 0.0793, 0.1566$  and  $0.3519$ , respectively.

solutions corresponding to these accretion solutions, are presented by  $M_j$  (9b, 9e, 9h, 9k) and  $v_j$  (9c, 9f, 9i, 9l). As  $\alpha$  increases  $x_s$  decreases, therefore increasing the pre-shock disc. Moreover, with decreasing  $x_s$ , the post-shock disc becomes smaller and hotter. So as  $x_s$  decreases, initially both  $\ell_s$  &  $\ell_{ps}$  will increase, but at around  $x_s \sim 100$ , further decrease of  $x_s$  will reduce  $\ell_s/\ell_{ps}$  and significantly increase  $\ell_{ps}$  (Fig. A1b). In Figs. 9a, d, g, j, increase of  $\alpha$ , causes a shift of  $x_s = 125.896 \rightarrow 8.5741$ . Consequently,  $\ell_{ps}$  increases from  $0.0054 \rightarrow 0.2337$ . The resulting jets are accelerated and the terminal velocity increases from  $v_\infty = 0.0534 \rightarrow 0.3519$  as shock shifts from  $x_s = 125.896 \rightarrow 8.5741$ , with the corresponding change in luminosity. By considering the relative proportions of post-shock and pre-shock radiations, decrease of  $x_s$  with increasing  $\alpha$  resembles the disc to move from hard state to hard intermediate state, and simultaneously the jet becomes stronger and faster (both  $v_\infty$  and  $R_{\dot{m}}$  increases). In Fig. 10a-c, we show the comparison of shock parameter space ( $E - \lambda_0$ ) of the accretion disc without massloss (dotted, online red) and with massloss but disc parameter  $\beta \dot{m}^2 = 0.001$  (long dashed, online black) and  $\beta \dot{m}^2 = 0.01$  (dashed, online blue), and for various viscosity parameter  $\alpha = 0$  (Fig. 10a),  $\alpha = 0.1$  (Fig. 10b) and  $\alpha = 0.2$  (Fig. 10c). It is to be noted, that the bounded regions in  $E - \lambda_0$  parameter space, show the parameters for steady state shocks to occur, but non-steady shocks still exist outside the bounded region. The parameter space shrinks when massloss is considered, because with massloss, the post-shock pressure decreases, and the entire range for which steady shock may have existed in absence of jets, will not be able to satisfy the momentum balance across the shock front. Moreover, shocks seem to exist for fairly high viscosity and in presence of massloss.

#### 4 DISCUSSION AND CONCLUSION

Our main focus in this paper has been to study radiative and thermal driving of bipolar jets from dissipative accretion disc. The thermal driving is determined by the thermal energy of the jet base or the post-shock region. In other words, hotter the post-shock region, faster will be the jet. However, the thermal energy in the inner disc though hot, but cannot produce jets with  $v_\infty > 0.1$  (Chakrabarti 1999; Chattopadhyay & Das 2007; Kumar & Chattopadhyay 2013), for any realistic temperature ranges of the accretion disc. As has been explained in section 1, only thermally driven outflows can achieve terminal speeds of the order of the sound speed at the base. Radiative driving of jet is due to the momentum deposition of the accretion disc photons on to the shock driven jet. The issue of radiative acceleration of jets have been studied earlier



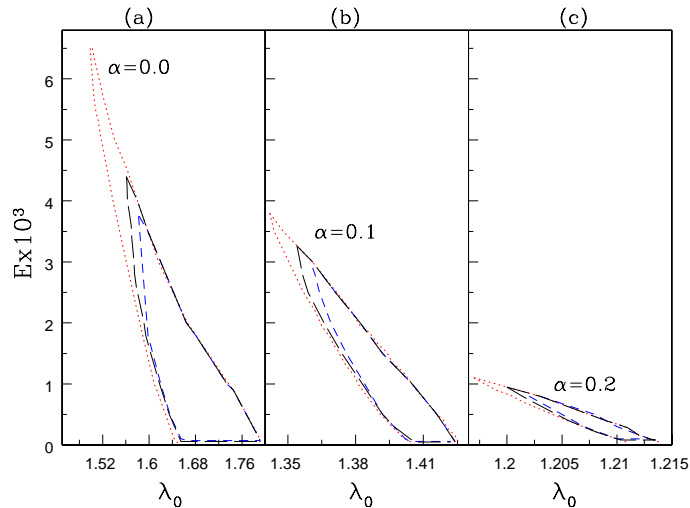


**Figure 10.** Shock parameter space or  $E - \lambda_0$  space for accretion, considered without massloss (dotted), and with massloss (dashed), and for  $\alpha = 0$  (a),  $\alpha = 0.1$  (b), and  $\alpha = 0.2$  (c).

(Chattopadhyay & Chakrabarti 2000, 2002), however, the jet base conditions in those works were assumed and were not self consistently obtained. In this paper, we do study the radiative acceleration of jets, but also by self-consistently solving the jet solution from the accretion disc solution itself. This is an exploratory study to investigate whether or not radiative driving is meaningful acceleration mechanism for jets. Radiative moments were calculated a posteriori from viscous accretion solutions.

We initially considered the post-shock luminosity ( $\ell_s$ ) as a parameter, and calculated the pre-shock radiation from the disc solution ( $a, \rho$ ) and by supplying  $\beta \dot{m}^2$ . Similar to Kumar & Chattopadhyay (2013), in this paper too, we find that with the increase of  $\alpha$  for disc solutions starting with same outer boundary condition, the shock location moves towards the horizon. As  $x_s$  decreases for fixed values of  $\ell_s$ , the jets are stronger and faster since the post-shock intensity increases (Figs. 6). For fixed values of  $\alpha$ , if  $\ell_s$  is increased, the jet is accelerated, as well as, more matter flows into the jet channel. The depleted post-shock flow causes  $x_s$  to decrease, in order to regain pressure balance across the shock. Since enhanced  $\ell_s$  increases the base velocity or  $v_{jb}$ , the jet sonic point decreases too.

The effect of pre-shock luminosity is quite different. Although pre-shock luminosity can accelerate as efficiently, as the post-shock radiation, however, since pre-shock radiation can ‘see’ mostly the supersonic branch of the jet, so neither  $R_{in}$  nor  $r_{jc}$  is affected appreciably. Therefore, one may conclude that post-shock radiation both accelerates and controls the mass outflow rate, pre-shock radiation increases the kinetic energy of the jet. And since for both pre-shock and post-shock radiations  $2\mathcal{F}_{r_j} \sim (\mathcal{E}_{r_j} + \mathcal{P}_{r_j})$  at  $r_j \sim \text{few} \times 100r_g$ , radiation drag effect is nullified at around that distance (Chattopadhyay *et al.* 2004; Chattopadhyay 2005). Which means faster jets can be obtained if enough radiation power can be supplied. And indeed we obtained terminal speeds of  $v_\infty \gtrsim 0.4$  for total disc luminosity  $\ell \sim 1$ . Although we have used  $\ell_s \leq 0.5$  (which is acceptable for luminous sources), but assigning arbitrary values of  $\ell_s$  may give wrong results, because  $\ell_s$  crucially depends on pre-shock radiation. So in Appendix 1, we have estimated  $\ell_s/\ell_{ps}(x_s)$  from correct radiative losses from a set of solutions of advective disc. We used this relation to estimate  $\ell_s$ , for given values of  $\ell_{ps}$  and  $x_s$ . We then increased  $\alpha$  for disc solutions starting with same  $E$  &  $\lambda_{inj}$ , and calculated simultaneous disc-jet solution. We showed that as  $\alpha$  is increased,  $x_s$  decreases and for reasons explained above, not only the disc moved from low intensity disc to brighter disc, but the jet became stronger and faster. Although, we have not considered the Keplerian disc component in our solution, but it resembles qualitatively, the transition of the disc from hard to intermediate hard states with associated strengthening of the jet from slow jets to faster and stronger jet, as has been reported in observations. We are still to include a few more physical processes in our disc-jet model, but our results qualitatively shows the correlation of disc spectral states and the jet states, as are observed in micro-quasars. Moreover, our result also indicates that, with multi-stage acceleration mechanism, truly relativistic jets from accretion disc are a distinct possibility.

## REFERENCES

- Becker, P. A., Das, S., Le, T., 2008, ApJ, 677, L93
- Biretta J. A., 1993, in Burgerella D., Livio M., Oea C., eds, Space Telesc. Sci. Symp. Ser., Vol. 6, Astrophysical Jets. Cambridge Univ. Press, Cambridge, p. 263
- Chakrabarti, S. K., 1989, ApJ, 347, 365
- Chakrabarti, S. K., Titarchuk, L., 1995, ApJ, 455, 623.
- Chakrabarti, S. K., 1996, ApJ, 464, 664
- Chakrabarti, S. K., 1999, A&A, 351, 185
- Chakrabarti, S. K., Manickam, S. G., 2000, ApJ, 531, L41
- Chakrabarti, S. K.; Das, S., 2004, MNRAS, 349, 649
- Chakrabarti, S. K., Mandal, S., 2006, ApJ, 642, L49.
- Chakrabarti, S. K., Debnath, D., Nandi, A., Pal, P. S., 2008, A&A, 489, L41
- Chakrabarti, S. K., Dutta, B. G., Pal, P. S., 2009, MNRAS, 394, 1463
- Chattopadhyay, I., Chakrabarti, S. K., 2000, Int. Journ. Mod. Phys., 9, 717.
- Chattopadhyay, I., Chakrabarti, S. K., 2002, MNRAS, 333, 454.
- Chattopadhyay, I., Chakrabarti, S. K., 2003, in Durouchoux Ph., Fuchs Y., and Rodriguez J., eds, New Views on Microquasars, Institut, d'Etudes, Scientifiques de Cargese, Corsica France, May 27-June 1, 2002, Center for Space Physics, Kolkata, India, p 126.
- Chattopadhyay, I., Das, S., Chakrabarti, S. K., 2004, MNRAS, 348, 846.
- Chattopadhyay, I., 2005, MNRAS, 356, 145
- Chattopadhyay, I.; Das, S., 2007, New A, 12, 454
- Chattopadhyay, I., 2008, in Chakrabarti S. K., Majumdar A. S., eds, AIP Conf. Ser. Vol. 1053, Proc. 2nd Kolkata Conf. on Observational Evidence of Black Holes in the Universe and the Satellite Meeting on Black Holes Neutron Stars and Gamma-Ray Bursts. Am. Inst. Phys., New York, p. 353
- Chattopadhyay, I., Chakrabarti, S. K., 2011, Int. Journ. Mod. Phys. D, 20, 1597
- Das, S., Chattopadhyay, I., Nandi, A., Chakrabarti, S. K., 2001, A&A, 379, 683
- Das, S.; Chattopadhyay, I., 2008, New A, 13, 549D.
- Das, S.; Becker, P. A.; Le, T., 2009 ApJ, 702, 649
- Doeleman, S., S., *et al.* 2012, Science, 338, 355.
- Feroci, M., Matt, G., Pooley, G., Costa, E., Tavani, M., Beloni, T., 1999, A&A, 351, 985.
- Fender R., Beloni, T., 2004, ARA&A, 42, 317
- Fender, R. P., Gallo, E., Russell, D., 2010, MNRAS, 406, 1425.
- Fukue, J., 1987, PASJ, 39, 309
- Fukue, J., 1996, PASJ, 48, 631
- Fukue, J., Tojyo, M., Hirai, Y., 2001, PASJ, 53, 555
- Fukumura, K., Tsuruta, S., 2004, ApJ, 611, 964
- Gallo, E., Fender, R. P., Pooley, G., G., 2003 MNRAS, 344, 60
- Gu, Wei-Min; Lu, Ju-Fu, 2004, ChPhL, 21, 2551
- Icke, V., 1980, AJ, 85(3), 329
- Icke, V., 1989, A&A216, 294
- Junor, W., Biretta, J. A., Livio, M., 1999, Nature, 401, 891
- Kumar R., Chattopadhyay I., 2013, MNRAS, 430
- Lanzafame, G., Cassaro, P., Schilliró, F., Costa, V., Belvedere, G., Zappalá, R. A., 2008, A&A, 482, 473
- Liang, E. P. T., Thompson, K. A., 1980, ApJ240, 271L
- Lu, J. F., Gu, W. M., & Yuan, F., 1999, ApJ, 523, 340
- Lynden-Bell D., 1978, Phys. Scr., 17, 185
- McHardy, I. M., Koerding, E., Knigge, C., Fender, R. P., 2006, Nature, 444, 730.
- Mandal, S., Chakrabarti, S., K., 2010, ApJ, 710, L147.
- Margon, B., 1984, ARA&A, 22, 507.
- Mihalas D., Mihalas B. W., 1984, Foundations of Radiation Hydrodynamics. Oxford Univ. Press, Oxford
- Miller-Jones, C. J. A., *et al.* , 2012, MNRAS, 421, 468.
- Mirabel I. F., Rodriguez L. F., 1994, Nat, 371, 46
- Molteni, D., Lanzafame, G., Chakrabarti, S. K., 1994, ApJ, 425, 161
- Molteni, D., Ryu, D., Chakrabarti, S. K., 1996a, ApJ, 470, 460
- Molteni, D., Sponholtz, H., Chakrabarti, S. K., 1996b, ApJ, 457, 805.
- Narayan, R., Kato, S., Honma, F., 1997, ApJ476, 49

- Nagakura, H., Yamada, S., 2009, ApJ, 696, 2026  
 Novikov, I. D.; Thorne, K. S., 1973, in Dewitt B. S., Dewitt C., eds, Black Holes. Gordon & Breach, New York, p. 343  
 Nishikawa, K. -I., Richardson, G., Koide, S., Shibata, K., 2005, ApJ, 625, 60  
 Paczyński, B. and Wiita, P.J., 1980, A&A, 88, 23.  
 Rushton, A., Spencer R., Fender, R., Pooley, G., 2010, A&A, 524, 29  
 Shakura, N. I.; Sunyaev, R. A., 1973, A&A, 24, 337S.  
 Shaposhnikov, N., Titarchuk, L., 2007, ApJ, 663, 445.  
 Shaposhnikov, N., Titarchuk, L., 2009, ApJ, 699, 453  
 Shapiro, S. L., Teukolsky, S. A., 1983, Black Holes, White Dwarfs and Neutron Stars, Physics of Compact Objects. Wiley-Interscience, New York. 66  
 Sikora M., Wilson D. B., 1981, MNRAS, 197, 529.  
 Sunyaev, R. A., Titarchuk, L., 1980, A&A, 86, 121.  
 Titarchuk, L., G., & Fiorito, R. 2004, ApJ, 612, 988.  
 Vadawale, S., Rao, A. R., Nandi, A., Chakrabarti, S. K., 2001, A&A, 370, L17.

## APPENDIX A: ESTIMATION OF POST-SHOCK LUMINOSITY FROM PRE-SHOCK RADIATIONS

We consider a general radiative transfer model (Chakrabarti & Mandal 2006) which consists of two components, a Keplerian disc on the equatorial plane and a sub-Keplerian component on the top of the Keplerian disc. The Keplerian disc supplies the multi-colour black body photons and a fraction of that photons are inverse-Comptonized by post-shock region. The pre-shock sub-Keplerian disc emits radiation via bremsstrahlung and synchrotron process whereas the post-shock region produces the same as in pre-shock along with the Comptonization of the local and intercepted soft photons. We calculate the radiation spectrum of accretion disc using the viscous transonic shocked solution for a given outer boundary condition  $E = 0.001$ ,  $\lambda_{inj} = 18.592$  at  $x_{inj} = 10^4$ . For a given value of  $\alpha$ , a shock is formed at  $x_s$ . The frequency integrated pre-shock and post-shock luminosity is then calculated. It has been shown in (Kumar & Chattopadhyay 2013) that for the same set of boundary conditions,  $x_s$  decreases if  $\alpha$  is increased. In our case for a range of  $0.0091 \leq \alpha \leq 0.01$ , for flows starting with the same injection values mentioned above, the shock location changes from  $x_s = 131 \rightarrow 7.8$  (Fig. A1a). We calculate the ratio of post-shock to pre-shock luminosity  $\ell_s/\ell_{ps}$  for different values of  $x_s$  in the range mentioned above and it has been plotted by dots in Fig. (A1b). In Fig. A1c we plot the associated variation in photon index, which shows the spectra softens as shock moves inward. The ratio ( $\ell_s/\ell_{ps}$ ) increases initially as the shock move inward, reaching a maximum value and then decreases sharply. This behaviour is due to fact that initially as shock moves inward both post-shock temperature and density increases and hence post-shock luminosity increases but as shock reaches closer to central object the pre-shock luminosity  $\ell_{ps}$  increases and the increased supply of pre-shock photons cools down the post-shock flow, and therefore the ratio would decrease too. We have fitted a polynomial through the model data points and this general behaviour of  $\ell_s/\ell_{ps}$  with  $x_s$  is used to calculate  $\ell_s$  for given value of  $\ell_{ps}$ .

The fitted polynomial for the relation between post-shock and pre-shock disc luminosity is,

$$f(x_s) = -0.659234 + 0.127851 x_s - 0.00043 x_s^2 - 1.13 \times 10^{-6} x_s^3, \quad (\text{A1})$$

where,  $f(x_s)$  is the fitted function for  $\ell_s/\ell_{ps}$ .

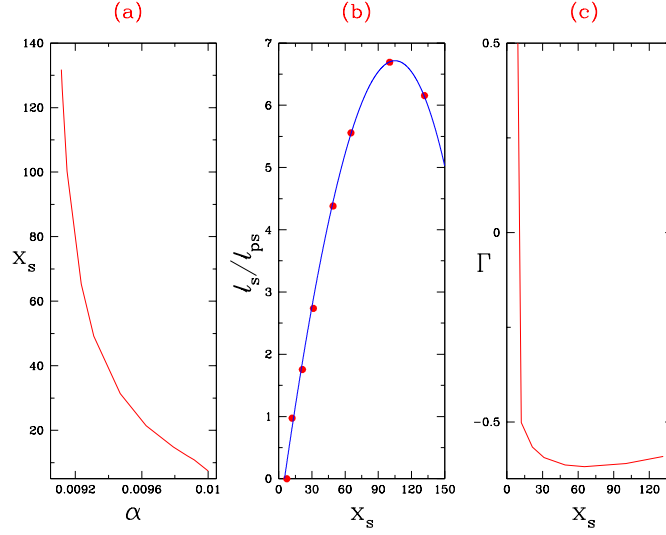


**Figure A1.** Variation of (a) shock location( $x_s$ ) with disc viscosity parameter( $\alpha$ ), and (b) ratio of  $\ell_s/\ell_{ps}$  with shock locations, and (c) the photon index  $\Gamma$  for the same injection values  $E = 0.001$ ,  $\lambda_{inj} = 18.592$  at disc outer boundary,  $x_{inj} = 10^4$  but varying viscosity parameter( $\alpha$ ) from 0.0091 to 0.01. In plot (b) dot points are actual data points and solid line is the fitted polynomial.